Available online at www.sciencedirect.com
SCIENCE DIRECT®
International Journal of Heat and Mass Transfer 49 (2006) 2372–2380
International Journal of HEAT and MASS TRANSFER
www.elsevier.com/locate/ijhmt

Stability of natural convection in an inclined square duct with perfectly conducting side walls

Takahiro Adachi *

Department of Mechanical Engineering, Akita University, 1-1 Tegata-Gakuen, Akita 010-8502, Japan

Received 12 May 2004; received in revised form 9 March 2005
Available online 20 February 2006

Abstract

We have performed three-dimensional linear stability analyses for natural convection in an inclined square duct. The duct is heated from the bottom, while the lateral walls are assumed to be perfectly thermal conducting. Three-dimensional transverse rolls whose axes are normal to the axis of the duct occur from the motionless state when the Rayleigh number exceeds a critical value and the duct is placed horizontally ($\theta = 0°$). However, it is found that when the duct is placed inclined ($\theta = 0.01°$), a two-dimensional longitudinal roll which is unchanged in the axis of the duct occurs and is stable if the Rayleigh number is small.

Keywords: Stability; Natural convection; Spectral element method; Critical Rayleigh number; Inclined square duct; Eigenvalue problem

1. Introduction

Natural convection in a long horizontal duct heated from the bottom appears in many practical and industrial devices such as heat exchangers, air conditioners and certain type of processing devices being used in various chemical plants. Fluid contained in the duct is in a motionless state if the duct is placed horizontally when the Rayleigh number is relatively small. Roll type natural convection occurs as a pitchfork bifurcation from the motionless state due to instability when the Rayleigh number exceeds a critical value. There are two kinds of the roll type convection to occur in the duct. One is longitudinal roll, referred to as L-roll hereafter, whose axis is parallel to that of the duct. The other is transverse roll, referred to as T-roll hereafter, whose axis is normal to that of the duct. It should be noted that the L-roll is two-dimensional flow unchanged in the axis of the duct, while the T-roll is three-dimensional one and periodic in the axis of the duct.

Davis [1] has examined the linear stability of the conduction state in a three-dimensional enclosure. He assumed a quasi-two-dimensional disturbance with two non-zero velocities depending on all spatial variables, and concluded that the T-rolls were predicted as a preferred mode of the convection in a rectangular enclosure like a duct. Later on, however, Davies-Jones [2] has pointed out that the quasi-two-dimensional disturbance did not exactly satisfy the linearized disturbance equations. Despite of such findings by Davies-Jones, the quasi-two-dimensional disturbance gives a close approximation of the preferred modes in some cases. Therefore, the T-roll convection occurs from the motionless state in the duct placed horizontally and heated from the bottom, and the resultant flow field is three-dimensional.

On the other hand, the L-roll convection appears in the duct under the assumption of two-dimensional flow fields. Critical conditions for onset of the L-roll convection from the motionless state have been evaluated for both insulating and conducting side walls by some researchers [3–6]. They calculated the critical Rayleigh numbers against the aspect ratio of the cross-section of the duct. In addition to the evaluation of the critical conditions, Adachi

* Tel.: +81 18 889 2306; fax: +81 18 837 0405.
E-mail address: adachi@ipc.akita-u.ac.jp

0017-9310/$ - see front matter © 2005 Elsevier Ltd. All rights reserved.
doi:10.1016/j.ijheatmasstransfer.2005.05.045

Nomenclature

g^*	gravitational acceleration
h^*	height and width of the duct
h_m	Lagrange interpolants through Gauss–Legendre–Lobatto points
$\tilde{h}_m$	Lagrange interpolants through Gauss–Legendre points
K	number of spectral element
N	truncation parameter of expansions
p	pressure
Pr	Prandtl number, $Pr = \nu^*/\kappa^*$
Ra	Rayleigh number, $Ra = \beta^* g^* h^{*3} \Delta T^*/\kappa^* \nu^*$
t	time
T	temperature
T_0^*	reference temperature
(u, v, w)	velocity components
(x, y, z)	rectangular co-ordinates
α	wave number in the x-direction
β^*	thermal expansion coefficient
ΔT^*	temperature difference between the lower and upper surfaces
κ^*	thermal diffusivity
ν^*	kinematic viscosity
λ	wave length $\lambda = 2\pi/\alpha$
ρ^*	density
θ	angle of inclination
$\omega = \omega_r + i\omega_i$	eigenvalue of the eigenvalue problem

Superscripts

c	critical
*	dimensional value

and Mizushima [9] have calculated the nonlinear steady solutions of L-roll after the bifurcation and investigated the secondary instability of the steady solutions. In the above analyses, the flow and temperature fields have been treated to be two-dimensional and unchanged in the axis of the duct. However, since a possible mechanism guaranteeing the two-dimensionality did not proposed, the results should be accepted as those of a mathematical model.

It is quite common that the duct is installed in an industrial devices inclined at certain degrees because of its accuracy limitation. Then, the natural convection always occurs even if the Rayleigh number is small enough. That is to say, there is no motionless state. The convection in the duct is the two-dimensional L-roll, because the balance between gravity and buoyancy force breaks uniformly along the axis of the duct. Therefore, the two-dimensionality seems to be valid in this case. The effect of an inclination of the duct has been considered by Cliffe and Winters [8]. They assumed that the side walls were insulated. It was shown that the pitchfork bifurcation became imperfect one. On the other hand, Mizushima and Adachi [9] have studied the effect of inclination on the bifurcation by weakly nonlinear stability theory. They derived an amplitude equation from a growth rate expansion method and explained the change of structures of the bifurcation. Furthermore, Ozoe et al. [10] have experimentally investigated a natural convection in an inclined square duct. They showed that the flow was the L-roll as the degree of inclination was greater than 10° from the horizontal, while multiple stable states were possible as the degree of inclination decreased below 10° from the horizontal, and a series of T-roll convection was eventually attained as the stable mode as the inclination approaches zero. Therefore, the flow fields changed between the L-roll and T-roll depending on the angle of inclination of the duct, but it is not apparent which convection between the L-roll and T-roll occurs if the duct is placed at an small angle of inclination.

In this paper, we investigate the stability of the natural convection in an inclined square duct. The duct is heated from the bottom and has perfectly conducting side walls. In order to clarify the preferred roll type for the case that the duct is placed at an small angle, we treat 0° and 0.01° as inclination angles. First, we calculate a nonlinear steady-state solution of the two-dimensional L-roll convection. Then, the three-dimensional linear stability theory is applied to the two-dimensional L-roll solution by using a spectral element method. The generalized eigenvalue problem of matrix form is constituted based on the linear stability theory. We evaluate the critical Rayleigh number where the L-roll and motionless state lose their stabilities to the three-dimensional disturbances, and also clarify the hydrodynamic nature of instability.

2. Mathematical formulation

2.1. Basic equations

Consider a fluid contained in an inclined square duct with each side-length h^* as shown in Fig. 1. Fig. 1(a) shows a part of infinitely long duct and Fig. 1(b) shows a cross-section of the duct. The x^*-axis is taken along one of the duct, the y^*-axis taken parallel to the bottom side and the z^*-axis taken perpendicular to the y^*-axis with origin O. The upper surface of the duct is isothermally cooled to keep the temperature $T_0^* - \Delta T^*/2$, while the lower one isothermally heated to keep $T_0^* + \Delta T^*/2$, where T_0^* is a reference temperature at $y^* = 0$ and its value is constant.

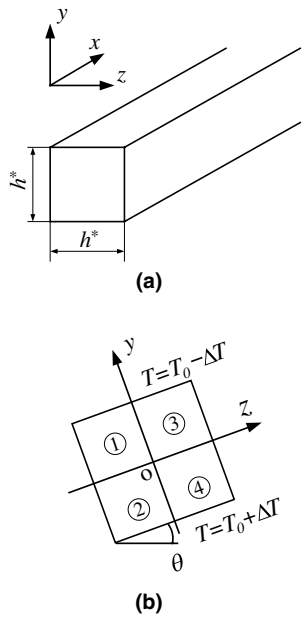

Fig. 1. Geometry and co-ordinates. The duct is placed at an angle θ of inclination. (a) A part of infinitely long duct. (b) Cross-section of the duct with 4 spectral element numbers.

We define non-dimensional quantities as follows

$$\begin{aligned} &x=\frac{x^*}{h^*}, \quad y=\frac{y^*}{h^*}, \quad z=\frac{z^*}{h^*},\\ &t=\frac{t^*}{(h^{*2}/\kappa^*)}, \quad u=\frac{u^*}{(\kappa^*/h^*)},\\ &v=\frac{v^*}{(\kappa^*/h^*)}, \quad w=\frac{w^*}{(\kappa^*/h^*)},\\ &p=\frac{p^*}{(\rho^*\kappa^{*2}/h^{*2})}, \quad T=\frac{(T^*-T_0^*)}{\Delta T^*}, \end{aligned} \tag{1}$$

where κ^* and ρ^* are the coefficient of thermal diffusivity and density of the fluid, respectively. We represent physical quantities with their dimensions by attaching a superscript * to them.

We assume that the flow is incompressible and the Boussinesq approximation is valid, where the approximation is applicable for sufficiently small temperature difference between the upper and lower surfaces. Then, the velocity (u,v,w), pressure p and temperature T are governed by the continuity, Navier–Stokes and energy equations as

$$\frac{\partial u}{\partial x}+\frac{\partial v}{\partial y}+\frac{\partial w}{\partial z}=0, \tag{2}$$

$$\frac{\partial u}{\partial t}+u\frac{\partial u}{\partial x}+v\frac{\partial u}{\partial y}+w\frac{\partial u}{\partial z} = -\frac{\partial p}{\partial x}+Pr\left(\frac{\partial^2 u}{\partial x^2}+\frac{\partial^2 u}{\partial y^2}+\frac{\partial^2 u}{\partial z^2}\right), \tag{3}$$

$$\frac{\partial v}{\partial t}+u\frac{\partial v}{\partial x}+v\frac{\partial v}{\partial y}+w\frac{\partial v}{\partial z} = -\frac{\partial p}{\partial y}+TRaPr\cos\theta+Pr\left(\frac{\partial^2 v}{\partial x^2}+\frac{\partial^2 v}{\partial y^2}+\frac{\partial^2 v}{\partial z^2}\right), \tag{4}$$

$$\frac{\partial w}{\partial t}+u\frac{\partial w}{\partial x}+v\frac{\partial w}{\partial y}+w\frac{\partial w}{\partial z} = -\frac{\partial p}{\partial z}+TRaPr\sin\theta+Pr\left(\frac{\partial^2 w}{\partial x^2}+\frac{\partial^2 w}{\partial y^2}+\frac{\partial^2 w}{\partial z^2}\right), \tag{5}$$

$$\frac{\partial T}{\partial t}+u\frac{\partial T}{\partial x}+v\frac{\partial T}{\partial y}+w\frac{\partial T}{\partial z}=\frac{\partial^2 T}{\partial x^2}+\frac{\partial^2 T}{\partial y^2}+\frac{\partial^2 T}{\partial z^2} \tag{6}$$

where Ra and Pr are the Rayleigh number and the Prandtl number, respectively, which are defined as

$$Ra=\frac{\beta^* g^* h^{*3}\Delta T^*}{\kappa^* \nu^*}, \quad Pr=\frac{\nu^*}{\kappa^*} \tag{7}$$

where β^*, ν^* and g^* are the coefficients of thermal expansion, kinematic viscosity of the fluid and gravitational acceleration. The value of the Prandtl number is fixed as $Pr=7$ throughout this paper.

We assume that all boundaries are rigid, therefore the velocity is zero on the wall. In addition to the velocity, the upper surface of the duct is isothermally cooled, while the lower one isothermally heated. For the lateral walls, we consider a thermally conducting state. Then the boundary conditions are written as

$$u=v=w=0, \quad T=\frac{1}{2}, \quad \text{at } y=-\frac{1}{2}, \tag{8}$$

$$u=v=w=0, \quad T=-\frac{1}{2}, \quad \text{at } y=\frac{1}{2}, \tag{9}$$

$$u=v=w=0, \quad T=-y, \quad \text{at } z=\pm\frac{1}{2}. \tag{10}$$

2.2. Steady-state equations for longitudinal roll

We calculate a nonlinear steady-state solution to study its linear stability. Now we focus ourselves on the L-roll convection unchanged in the axial x-direction of the duct which includes the motionless state. The nonlinear steady-state solution is expressed as $(\overline{V}(y,z),\ \overline{W}(y,z),\ \overline{T}(y,z),\ \overline{P}(y,z))$. Substituting the expressions into Eqs. (2)–(6) and dropping the terms including the operator $\partial/\partial t$, we obtain the following two-dimensional steady-state equations as

$$\frac{\partial \overline{V}}{\partial y}+\frac{\partial \overline{W}}{\partial z}=0, \tag{11}$$

$$\overline{V}\frac{\partial \overline{V}}{\partial y}+\overline{W}\frac{\partial \overline{V}}{\partial z}=-\frac{\partial \overline{P}}{\partial y}+\overline{T}RaPr\cos\theta+Pr\left(\frac{\partial^2 \overline{V}}{\partial y^2}+\frac{\partial^2 \overline{V}}{\partial z^2}\right), \tag{12}$$

$$\overline{V}\frac{\partial \overline{W}}{\partial y}+\overline{W}\frac{\partial \overline{W}}{\partial z}=-\frac{\partial \overline{P}}{\partial z}+\overline{T}RaPr\sin\theta+Pr\left(\frac{\partial^2 \overline{W}}{\partial y^2}+\frac{\partial^2 \overline{W}}{\partial z^2}\right), \tag{13}$$

$$\overline{V}\frac{\partial \overline{T}}{\partial y}+\overline{W}\frac{\partial \overline{T}}{\partial z}=\frac{\partial^2 \overline{T}}{\partial y^2}+\frac{\partial^2 \overline{T}}{\partial z^2}. \tag{14}$$

The boundary conditions for $(\overline{V}(y,z), \overline{W}(y,z), \overline{T}(y,z))$ are the same as Eqs. (8)–(10).

2.3. Linear disturbance equations

All the steady-state solutions obtained from Eqs. (11)–(14) are not stable. We investigate the linear stability of the steady solutions by adding disturbances to them and by observing the time dependence for the disturbances. Then, the velocity, temperature and pressure are expressed as the sum of the steady solution $(\overline{V}, \overline{W}, \overline{T}, \overline{P})$ and the disturbance defined as

$$\begin{pmatrix} u \\ v \\ w \\ T \\ p \end{pmatrix} = \begin{pmatrix} 0 \\ \overline{V} \\ \overline{W} \\ \overline{T} \\ \overline{P} \end{pmatrix} + \begin{pmatrix} \tilde{u} \\ \tilde{v} \\ \tilde{w} \\ \tilde{T} \\ \tilde{p} \end{pmatrix} \exp[\mathrm{i}(\alpha x - \omega t)] \tag{15}$$

where α is a wave number and ω is a complex frequency. The real part ω_r and the imaginary part ω_i denote the frequency and the linear growth rate of the disturbance, respectively. The steady solution is unstable if $\omega_\mathrm{i} > 0$ and the disturbance grows with time. The disturbance with $\alpha = 0$ forms the two-dimensional flow field, while one with $\alpha \neq 0$ forms the three-dimensional one.

Substituting Eq. (15) into Eqs. (2)–(6), then subtracting the steady-state equations from the resultant equations and dropping the nonlinear terms of the disturbance, we obtain the following linearized equations for the disturbance as

$$\mathrm{i}\alpha\tilde{u} + \frac{\partial\tilde{v}}{\partial y} + \frac{\partial\tilde{w}}{\partial z} = 0, \tag{16}$$

$$-\mathrm{i}\omega\tilde{u} + \overline{V}\frac{\partial\tilde{u}}{\partial y} + \overline{W}\frac{\partial\tilde{u}}{\partial z} = \mathrm{i}\alpha\tilde{p} + Pr\left\{(\mathrm{i}\alpha)^2\tilde{u} + \frac{\partial^2\tilde{u}}{\partial y^2} + \frac{\partial^2\tilde{u}}{\partial z^2}\right\}, \tag{17}$$

$$\begin{aligned} &-\mathrm{i}\omega\tilde{v} + \overline{V}\frac{\partial\tilde{v}}{\partial y} + \tilde{v}\frac{\partial\overline{V}}{\partial y} + \overline{W}\frac{\partial\tilde{v}}{\partial z} + \tilde{w}\frac{\partial\overline{V}}{\partial z} \\ &= -\frac{\partial\tilde{p}}{\partial y} + \widetilde{T}RaPr\cos\theta + Pr\left\{(\mathrm{i}\alpha)^2\tilde{v} + \frac{\partial^2\tilde{v}}{\partial y^2} + \frac{\partial^2\tilde{v}}{\partial z^2}\right\}, \end{aligned} \tag{18}$$

$$\begin{aligned} &-\mathrm{i}\omega\tilde{w} + \overline{V}\frac{\partial\tilde{w}}{\partial y} + \tilde{v}\frac{\partial\overline{W}}{\partial y} + \overline{W}\frac{\partial\tilde{w}}{\partial z} + \tilde{w}\frac{\partial\overline{W}}{\partial z} \\ &= -\frac{\partial\tilde{p}}{\partial z} + \widetilde{T}RaPr\sin\theta + Pr\left\{(\mathrm{i}\alpha)^2\tilde{w} + \frac{\partial^2\tilde{w}}{\partial y^2} + \frac{\partial^2\tilde{w}}{\partial z^2}\right\}, \end{aligned} \tag{19}$$

$$-\mathrm{i}\omega\widetilde{T} + \overline{V}\frac{\partial\widetilde{T}}{\partial y} + \tilde{v}\frac{\partial\overline{T}}{\partial y} + \overline{W}\frac{\partial\widetilde{T}}{\partial z} + \tilde{w}\frac{\partial\overline{T}}{\partial z} = \left\{(\mathrm{i}\alpha)^2\widetilde{T} + \frac{\partial^2\widetilde{T}}{\partial y^2} + \frac{\partial^2\widetilde{T}}{\partial z^2}\right\}. \tag{20}$$

The boundary conditions for $((\tilde{u}(y,z), \tilde{v}(y,z), \tilde{w}(y,z)))$ are the same as Eqs. (8)–(10). On the other hand, the boundary condition for $\widetilde{T}(y,z)$ is written as

$$\widetilde{T} = 0 \quad \text{at } y = \pm\frac{1}{2} \quad \text{and} \quad z = \pm\frac{1}{2}. \tag{21}$$

3. Numerical method

The numerical calculations are carried out by utilizing a spectral element method [11,12]. The spectral element method has both the generality of the finite element method and the accuracy of the classical spectral method.

In the spectral element method, the actual calculation domain is broken up into K elements. Here we break the domain into 4 elements such as (1) $0 \leqslant y \leqslant 0.5$, $-0.5 \leqslant z \leqslant 0$, (2) $-0.5 \leqslant y \leqslant 0$, $-0.5 \leqslant z \leqslant 0$, (3) $0 \leqslant y \leqslant 0.5$, $0 \leqslant z \leqslant 0.5$ and (4) $-0.5 \leqslant y \leqslant 0$, $0 \leqslant z \leqslant 0.5$ as shown in Fig. 1(b). Each element is mapped from the physical (y,z) space to the local $(\bar{y},\bar{z})$ coordinate system whose ranges are $[-1,1]$. For example, the coordinate transformation from y being of the length L^k and defined on the interval $[a^k,b^k]$ in the kth element to $\bar{y}$ is carried out by the following equation as

$$\bar{y} = \frac{2}{L^k}(y - a^k) - 1. \tag{22}$$

The velocity, temperature and pressure are expanded by high-order Lagrangian interpolants as

$$\begin{pmatrix} u^k(\bar{y},\bar{z}) \\ v^k(\bar{y},\bar{z}) \\ w^k(\bar{y},\bar{z}) \\ T^k(\bar{y},\bar{z}) \end{pmatrix} = \sum_{m=0}^{N}\sum_{n=0}^{N} \begin{pmatrix} u^k_{mn} \\ v^k_{mn} \\ w^k_{mn} \\ T^k_{mn} \end{pmatrix} h_m(\bar{y})h_n(\bar{z}), \tag{23}$$

$$p^k(\bar{y},\bar{z}) = \sum_{m=1}^{N-1}\sum_{n=1}^{N-1} p^k_{mn}\tilde{h}_m(\bar{y})\tilde{h}_m(\bar{z}), \quad (k = 1,\ldots,4). \tag{24}$$

where h_m is the Nth order Lagrange interpolants through $(N+1)$ Gauss–Legendre–Lobatto points in the kth element and $\tilde{h}_\mathrm{m}$ is the $(N-2)$th order interpolants through $(N-1)$ Gauss–Legendre points in the kth element.

Substituting the expansions of Eqs. (23) and (24) into the weak forms of both the steady-state and disturbance equations and also using the Galerkin method, we obtain a set of algebraic equations for the coefficients of the expansions. We use a mapping array method [12] to construct the system matrix from the element matrices. The set of algebraic equations for the steady solution are solved numerically by the Newton–Raphson method. On the other hand, the set of algebraic equations for the stability of the steady solution constitutes a generalized eigenvalue problem in a matrix form as

$$\mathbf{Aa} = \omega\mathbf{Ba} \tag{25}$$

where $\mathbf{a}$ is a vector of expansion coefficients, and $\mathbf{A}$ and $\mathbf{B}$ are the matrices arising from the right-hand side and left-hand side of Eqs. (16)–(20), respectively. The eigenvalue ω, with maximum imaginary part, determines the stability characteristics of the steady solution and the corresponding eigenvector represents the flow and temperature fields of the disturbance. The eigenvalue problem is solved numerically by a QR method. Stability analyses based on the spectral element method and constituting the eigenvalue

problem have been carried out by Adachi and Uehara [13] for flow in a complex geometry.

All the numerical calculations are done with double precisions and the values of the truncation parameters in Eqs. (23) and (24) are taken as $N = 8$. The results are confirmed to be valid up to four significant digits by changing the parameters.

4. Results

4.1. Nonlinear steady-state solutions

We adopt a velocity v_0 in the y-direction at $(y,z) = (0,1/4)$ as a physical quantity which characterizes the nonlinear steady solution. The velocity v_0 is plotted against Ra in Fig. 2 for both $\theta = 0°$ and 0.01°. There are three solutions for $\theta = 0°$ in Fig. 2(a), which are represented by OA, PB and PC. The line OA indicates the motionless state due to $v_0 = 0$ which means that there is no natural convection. As a result of a pitchfork bifurcation, the L-roll convections PB and PC appear at the critical point P of $Ra_P = 5011.7$ [9,7]. Namely, under the assumption of the two-dimensionality, there is no natural convection for $Ra < Ra_P$ and the motionless state becomes unstable for $Ra > Ra_P$. The stable convection branches PB and PC appear for $Ra > Ra_P$. The direction of the convective motion for PB and PC is opposite each other and cannot be predicted in a deterministic manner but is selected by chance. On the other hand, there are three L-roll convective solutions for the case of $\theta = 0.01°$ in Fig. 2(b). One is a smooth transition branch OD which extends from $Ra = 0$, therefore there is no motionless state in this case. The others are saddle-node branches SE and SF which join at a saddle-node point S of $Ra_S = 5042.0$. It is recognized that the branch SE is a metamorphose of PA for $\theta = 0°$ and is always unstable. We can see from the figure that the bifurcation is the imperfect pitchfork one for $\theta = 0.01°$. The direction of the convective motion is the same with that of the inclination of the duct for the solution of OD, and is opposite to one of SE and SF.

The flow and temperature fields of the steady-state solutions for $Ra = 6000$ and $\theta = 0°$ and 0.01° are shown in Fig. 3 as an example, which corresponds to the points denoted by Q and R in Fig. 2. There is one big circulation in the center of the flow field for $Ra = 6000$ in Fig. 3(a). The direction of circulation is counter-clockwise because the value of v_0 at Q and R is positive, so the flow fields seem to be skewed to the counter-clockwise direction. The corresponding temperature field is depicted in Fig. 3(b). The right-hand side has a local maximum temperature and the other a local minimum temperature because the global circulation is in the counter-clockwise direction. The flow and temperature fields for $Ra = 6000$ and $\theta = 0.01°$ are also skewed to the direction of the circulation as depicted in Fig. 3(c) and (d).

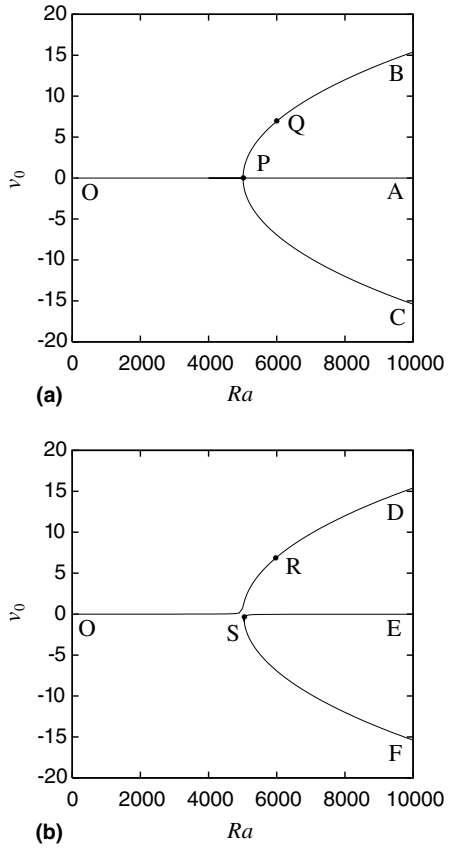

Fig. 2. Bifurcation diagram v_0 against Ra. (a) OA, PB and PC for $\theta = 0°$, (b) OD, SE and SF for $\theta = 0.01°$.

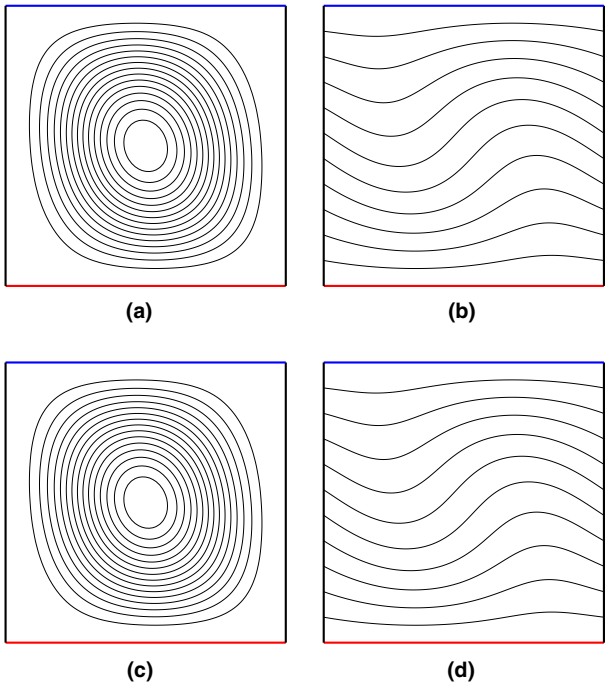

Fig. 3. Flow and temperature fields for $Ra = 6000$. (a) and (c) Streamlines, (b) and (d) Contour-lines for temperature. (a) and (b) for $\theta = 0°$, (c) and (d) for $\theta = 0.01°$.

4.2. Linear stability

All the steady nonlinear solutions obtained previously are not stable. We investigate the three-dimensional linear stability of the steady L-roll solutions including the motionless state which is indicated by OA, PB, OD and SF in Fig. 2. It should be noted that the stability characteristics of PC for $\theta = 0°$ are the same as one of PB, while SE for $\theta = 0.01°$ is a metamorphose of PA for $\theta = 0°$ and is always unstable. Therefore, we do not examine the stability of the steady solutions of PC and SE. We will show the linear neutral stability curves against the wave number α. The maximum linear growth rate ω_i changes from a negative value to a positive one across the neutral curve. When the neutral curve has a local minimum, we define the point as the critical Rayleigh number Ra_c and the critical wave number α_c.

Fig. 4(a) shows the neutral curve obtained from stability analyses for the motionless state of $\theta = 0°$ which corresponds to the branch OA in Fig. 2. It seems that the instability modes which work to destabilize the motionless state exchange themselves near the point of $\alpha = 1.25$. It is evident that the instability mode for $\alpha < 1.25$ is arisen from one of $\alpha = 0$. This means that the mode inherits the characteristics of L-roll. On the other hand, the mode for $\alpha > 1.25$ has characteristics of the T-rolls, which should be confirmed in the later section from the flow and temperature fields. The critical Rayleigh number of OA for the three-dimensional disturbance is being evaluated as $Ra_c = 2936.4$ at $\alpha_c = 3.14$, which is less than the critical value of $Ra_P = 5011.7$ for the two-dimensional disturbance ($\alpha = 0$). The frequency of the disturbance ω_r is zero, therefore the principle of exchange of stabilities are valid [14], and the bifurcated solution is a steady convection. In addition, we investigate the linear stability of the steady L-roll solution PB and show the neutral curve in Fig. 4(b) against the wave number. It is seen that the neutral curve is constant as $Ra = Ra_P = 5011.7$ for $\alpha > 1.45$. This implies that the growth rate is always positive value for $\alpha > 1.45$ and $Ra > Ra_P$, and the L-roll solution for $\theta = 0°$ is unstable for the three-dimensional disturbances.

Next, we show the neutral curve against the wave number for OD of $\theta = 0.01°$ in Fig. 5(a). As is evident from this figure, the neutral curve changes at $\alpha \sim 1.25$, but the instability modes does not exchange in this case as shown in the later section. The critical Rayleigh number for OD is being evaluated as $Ra_c = 2941.6$ at $\alpha_c = 3.38$. The frequency of the disturbance is zero also in this case. The neutral curve for the steady L-roll solution SF against the wave number is shown in Fig. 5(b). Again, the neutral curve is constant as $Ra = Ra_S = 5042.0$ for $\alpha > 1.44$, which means that the solution SF is unstable. As we have shown, the L-roll for $\theta = 0.01°$ is stable for $Ra < 2941.6$, while the L-roll is always unstable for $\theta = 0°$. Therefore, we can conclude that the structure of the flow fields are quite different depending

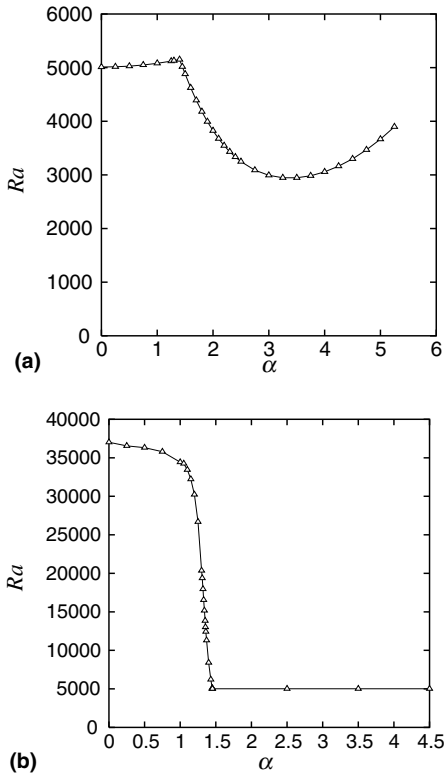

Fig. 4. The linear neutral stability curves for $\theta = 0°$. (a) The curve for the motionless state OA. (b) The curve for the L-roll branch PB.

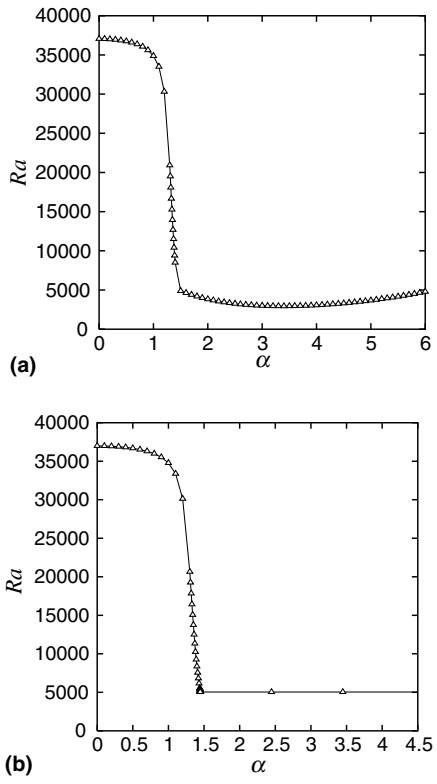

Fig. 5. The linear neutral stability curves for $\theta = 0.01°$. (a) The curve for the smooth transition branch OD. (b) The curve for the saddle-node branch SE.

on the angle of inclination, even if the angle is small such as 0.01°.

It is evident that the perfect pitchfork bifurcation occurs from the motionless state OA for $\theta = 0°$ at $Ra_c = 2936.4$ and $\alpha_c = 3.14$, where OA loses its stability for the three-dimensional disturbances. After that, the two branches of T-rolls whose circulation is in opposite direction each other bifurcate from the critical point, although we are regretfully unable to calculate the three-dimensional roll solutions in this study. The structure of the bifurcation $\theta = 0.01°$ seems to be invariant for the three-dimensional disturbance and also the perfect pitchfork one. Namely, the smooth transition L-roll branch OD loses its stability at $Ra = 2941.6$ and $\alpha = 3.38$ for the three-dimensional disturbance, and the two new branches stem from the point. It is expected that the resultant flow and temperature fields from the critical points are super-posed fields between L-roll and T-rolls. The robustness of the bifurcation structure is quite different from the case of steady solutions of the L-roll as seen earlier in Section 4.1.

4.3. Flow and temperature fields of disturbances

Flow and temperature fields of the disturbance on the neutral curve are obtained from the eigenvector for the eigenvalue problem. We show the flow and temperature fields for $\theta = 0°$ in Fig. 6. The range of the x-direction in the figure is $0 < x < 3\lambda$, where $\lambda = 2\pi/\alpha$ is a wave length in the x-direction of the disturbance. Streak-lines on the neutral curve at $\alpha = 1.0$ and $Ra = 5080.2$ as seen in Fig. 6(a) appears a roll type convection with the axis parallel to the axis of the duct, which is somewhat modified along the axis due to $\alpha \neq 0$. It is confirmed that the disturbance for $\alpha < 1.25$ inherits the characteristics of two-dimensional L-roll solution as mentioned previously. The corresponding temperature field by the contour-lines is depicted in Fig. 6(b), where the axis of the contour-lines seems to be along the axis of the duct. Fig. 6(c) and (d) show the streak-lines and contour-lines of the temperature at the criticality for the motionless state. In this case, the axes of the rolls are perpendicular to the axis of the duct. Therefore, the resultant fields from the bifurcation due to the three-dimensional disturbances are the T-roll convection.

Streak-lines and contour-lines of the temperature for $\theta = 0.01°$ on the neutral curve at $\alpha = 0.1$ and $Ra = 37037$ as seen in Fig. 7(a) and (b) also appear a roll type convection. Therefore, it is confirmed that the disturbance for $\alpha < 1.25$ inherits the characteristics of two-dimensional L-roll solution. The streak-lines and contour-lines of the temperature for $\theta = 0.01°$ at the criticality are depicted in Fig. 7(c) and (d), where $\alpha = 3.38$ and $Ra = 2941.6$. As the

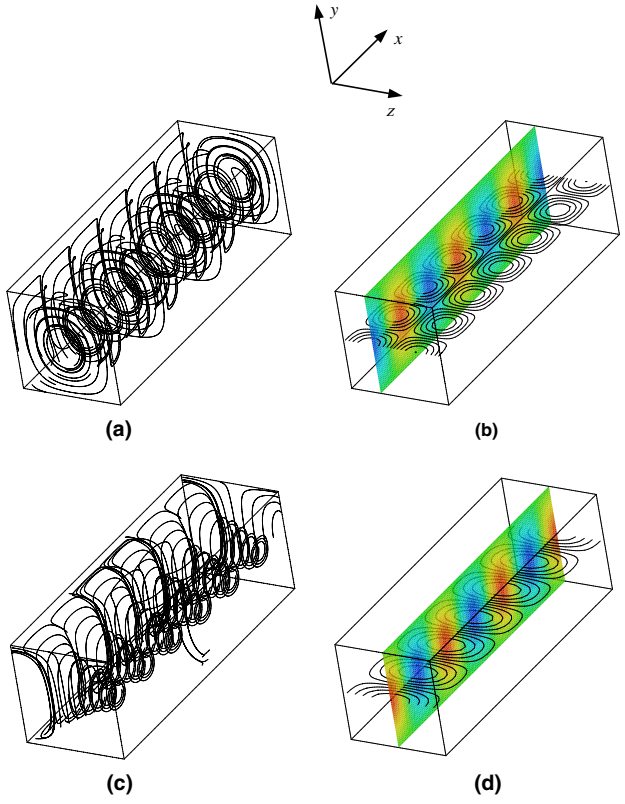

Fig. 6. Flow and temperature field for $\theta = 0°$, where the phase is arbitrary. (a) and (c) Flow fields. (b) and (d) Temperature fields. (a) and (b) Fields at $Ra = 5080.2$ and $\alpha = 1.0$. (c) and (d) Fields at the critical point.

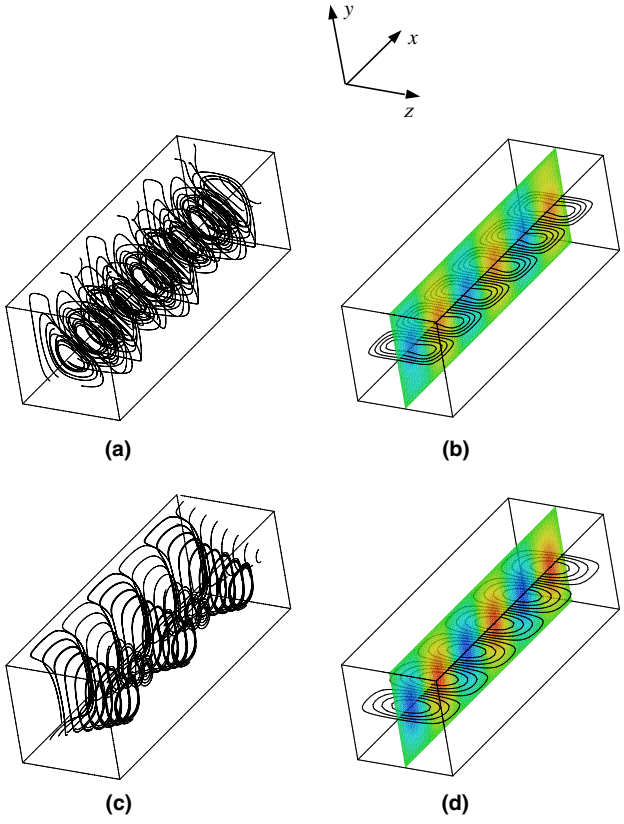

Fig. 7. Flow and temperature field for $\theta = 0.01°$, where the phase is arbitrary. (a) and (c) Flow fields. (b) and (d) Temperature fields. (a) and (b) Fields at A at $Ra = 37037$ and $\alpha = 0.1$. (c) and (d) Fields at the critical point.

axes of the rolls are perpendicular to the axis of the duct, the fields of the disturbances are T-roll convection. It is expected that the resultant flow and temperature fields from the critical points are super-posed fields between L-roll and T-rolls.

We can explain the reason why the instability modes abruptly change around $\alpha \sim 1.25$ as follows. The axis of convection is modulated for the case of $\alpha \neq 0$, and the vorticity turns to the different direction along the modulation as seen in Fig. 8(a). It has been shown that axes approach each other with aligning their vorticity anti-parallel from a localized induction approximation theory [15,16]. When α is small, the induction velocity between the axes is also small. So the axes balance each other and keep the inherent two-dimensionality from $\alpha = 0$. However, when α is larger and the corresponding wave length is shorter, the induction velocity becomes larger. Once the wave length is shorter than a certain critical length, the axes come to arrange anti-parallel at a stroke as seen in Fig. 8(b). It is thought that the limit of wave number is $\alpha \sim 1.25$ and the neutral curves abruptly change around the point.

The axes of the T-rolls is almost parallel to the horizontal if the angle of inclination is small. As the angle increases, however, the direction of the axes tends to the vertical, which leads to unrealistic flow and temperature fields. This implies that the super-posed flow can be realized within the limits of small angels of inclination. It is comparable with the result of Ozoe et al. [10] who showed that there was a transient flow regime for angle between 0° and 10°.

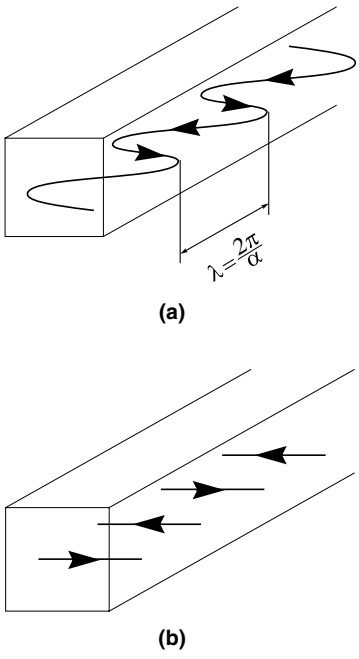

Fig. 8. Schematic figure to explain the exchange of instability modes. (a) Two-dimensional mode with axial modulations and (b) Three-dimensional mode with anti-parallel axes.

5. Concluding remarks

We have calculated the two-dimensional nonlinear steady solutions in an inclined square duct and have performed the three-dimensional stability analyses for the steady solutions based on the linear stability theory. It is widely recognized that the assumption of two-dimensional flow fields is not appropriate as a model of convection in the duct which is placed horizontally and is heated from the bottom. However, the situation have been quite different when the duct is placed at an angle from the horizontal plane even if the angle is only 0.01°. We summarize the main conclusions as follows and show the schematic figure of the obtained results in Fig. 9.

1. Three-dimensional T-rolls whose axes are normal to the axis of the duct occur from the motionless state when the Rayleigh number exceed a critical value $Ra_c = 2936.4$ and $\alpha_c = 3.14$ which is indicated by A in Fig. 9, where the duct is placed horizontally ($\theta = 0°$). However, it is found that only 0.01° inclination leads to the two-dimensional L-roll flow from the T-roll flow field for $\theta = 0°$ and the L-roll is stable up to the critical Rayleigh number. We have evaluated the critical Rayleigh number and the critical wave number $Ra_c = 2941.6$ and $\alpha_c = 3.38$ where the L-roll becomes unstable for the three-dimensional disturbance which is indicated by B in Fig. 9.
2. It is well known that the pitchfork bifurcation is structurally unstable to some perturbations in the system. Even a small angle of inclination as $\theta = 0.01°$ affects the bifurcation structure for the L-roll solutions under the assumption of two-dimensionality, and the perfect pitchfork bifurcation becomes imperfect one. On the other hand, it is now apparent that the pitchfork bifurcation for three-dimensional disturbances is structurally stable for the angle of inclination.
3. The resultant flow field from the motionless state for the three-dimensional disturbances in the case of $\theta = 0°$ is

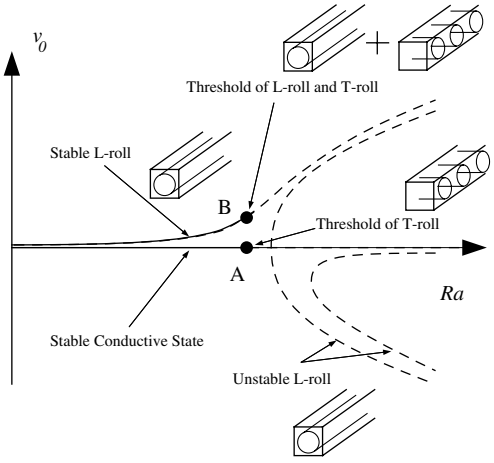

Fig. 9. Schematic figure of the obtained results. Stable and unstable solutions are indicated by the solid and dashed lines, respectively.

the T-roll convection which occur the critical point A in Fig. 9. On the other hand, the resultant flow field from the critical point B seen in Fig. 9 for the case of $\theta = 0.01°$ is the super-posed flow between L-roll and T-rolls.

Acknowledgements

The author is thankful to Mr. S. Imai, Akita university, for his help of calculation and drawing figures. A part of the results in this work were obtained using supercomputing resources at Information Synergy Center, Tohoku University. We also thank Mr. A. Otsuka for his helpful comments.

References

[1] S.H. Davis, Convection in a box:linear theory, J. Fluid Mech. 30 (1967) 465–478.
[2] R.P. Davies-Jones, Thermal convection in an infinite channel with no-slip sidewalls, J. Fluid Mech. 44 (1970) 695–704.
[3] U. Kurzweg, Convective instability of a hydromagnetic fluid within a rectangular cavity, Int. J. Heat Mass Transfer 8 (1965) 35–41.
[4] K.A. Cliffe, K.H. Winters, The use of symmetry in bifurcation calculations and its application to the Benard problem, J. Comput. Phys. 67 (1986) 310–326.
[5] N.Y. Lee, W.W. Schultz, J.P. Boyd, Stability of fluid in a rectangular enclosure by spectral method, Int. J. Heat Mass Transfer 32 (1989) 513–520.
[6] J. Mizushima, Onset of the thermal convection in a finite two-dimensional box, J. Phys. Soc. Jpn. 64 (1995) 2420–2432.
[7] T. Adachi, J. Mizushima, Stability of the thermal convection in a tilted square cavity, J. Phys. Soc. Jpn. 65 (1996) 1686–1698.
[8] K.A. Cliffe, K.H. Winters, A numerical study of the cusp catastrophe for Benard convection in tilted cavities, J. Comput. Phys. 54 (1984) 531–534.
[9] J. Mizushima, T. Adachi, Structural stability of the pitchfork bifurcation of thermal convection in a rectangular cavity, J. Phys. Soc. Jpn. 64 (1995) 4670–4683.
[10] H. Ozoe, H. Sayama, S.T. Churchill, Natural convection in an inclined square channel, Int. J. Heat Mass Transfer 17 (1974) 401–406.
[11] A.T. Patera, A spectral element method for fluid dynamics: laminar flow in a channel expansion, J. Comput. Phys. 54 (1984) 468–488.
[12] G.E. Karniadakis, S.J. Sherwin, Spectral/hp Element Methods for CFD, Oxford University Press, 1999, Section 2.
[13] T. Adachi, H. Uehara, Linear stability analysis of flow in a periodically grooved channel, Int. J. Numer. Method Fluids 41 (2003) 601–613.
[14] P.G. Drazin, W.H. Reid, Hydrodynamic Stability, Cambridge University Press, 1981, Section 2.
[15] E.D. Siggia, Collapse and amplification of a vortex filament, Phys. Fluids 28 (1985) 794–805.
[16] S. Kida, H. Miura, T. Adachi, Flow structure visualization by a low-pressure vortex, in: J.C. Vassilicos (Ed.), Intermittency in turbulent flow, Cambridge University Press, 2001, pp. 262–276.